of a 2006 El Niño that was stronger (considerably weaker) than that of 2002/03 (1997/98).

b. Temperature

1) Sea surface temperature—R. W. Reynolds

SSTs for 2006 are shown as monthly fields interpolated from the weekly 1° OI analyses of Reynolds et al. (2002). All results presented here are depicted as anomalies defined as differences from a 1971–2002 climatological base period described by Xue et al. (2003).

The yearly average and standard deviation of the monthly anomalies are shown in Fig. 3.1. The anomalies are primarily positive resulting from overall global warming relative to the climatological base period. Three features dominate 2006. First, the average shows a strong positive anomaly signal in the North Atlantic and North Pacific between roughly 40° and 65°N. This is due to a boreal summer positive anomaly, which also occurred in 2003–06. However, in 2006, the summer anomaly in the Pacific was relatively weak compared with 2003–05. Second, in 2005 there was also a strong positive anomaly of roughly 1°C in the tropical North Atlantic (0°–30°N) while in 2006 it was smaller. Finally, a weak El Niño began to be evident in June (see section 4).

The zonally averaged monthly anomaly is shown for the Atlantic between 80°W and 20°E for 2000–06 in Fig. 3.2. Strong positive summer anomalies are shown north of 40°N beginning in 2003. The anomaly signals were the oceanic response to summer heat waves that helped reduce summer ice cover in the Arctic. The 2003 European summer heat wave corresponded to an especially strong positive SST anomaly. In addition, the 2005 spring and summer tropical North Atlantic positive anomalies are evident between 5° and 20°N in the figure and were smaller in 2006. The smaller anomalies in 2006 may partly explain the lower number of 2006 Atlantic hurricanes compared to 2005.

2) Heat content—G. C. Johnson, J. M. Lyman, and J. K. Willis

Storage and transport of heat in the ocean are central to such aspects of climate as El Niño (e.g.,

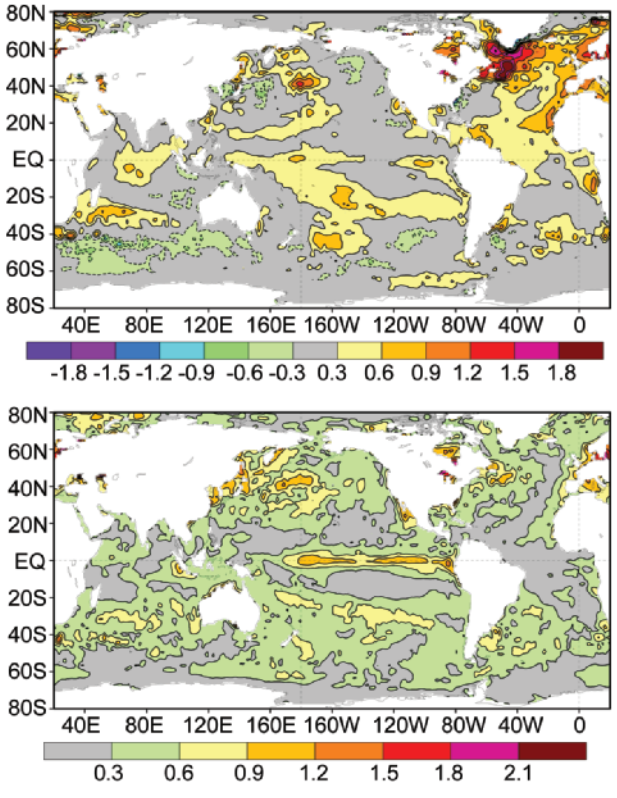

Fig. 3.1. Mean (top) and standard deviation (bottom) of monthly SST anomalies for 2006 on a 1° spatial grid. The anomalies are computed relative to a 1971–2000 base period. The contour interval is 0.3°C; the 0 contour is not shown. AVHRR satellite data are used.

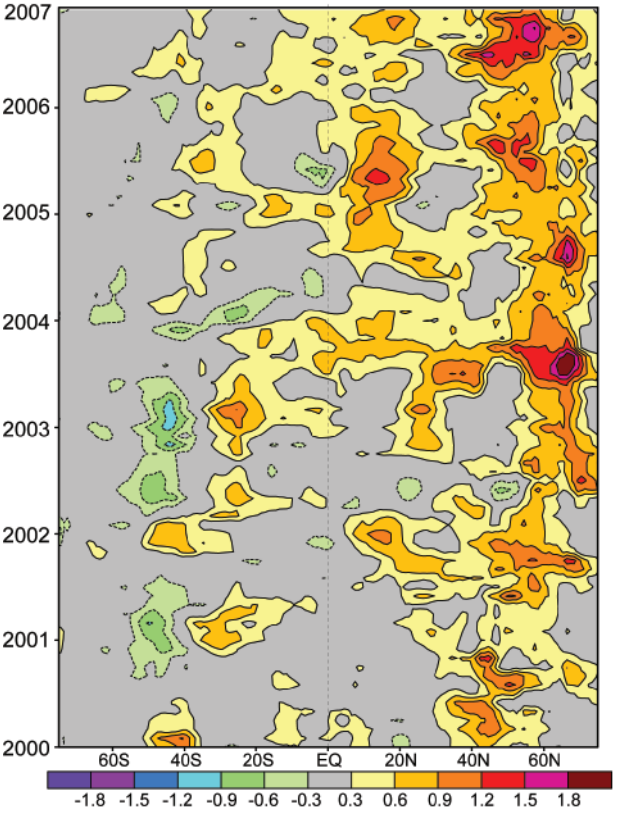

Fig. 3.2. Zonally averaged monthly SST anomalies for January 2000 through December 2006 for the Atlantic. The contour interval is 0.3°C; the zero contour is not shown. The anomalies are computed relative to a 1971–2000 base period.

Zebiak 1989), the North Atlantic Oscillation (e.g., Curry and McCartney 2001), hurricane seasons (e.g., Emanuel 2005), and global change (e.g., Levitus et al. 2005; Hansen et al. 2005). Here we discuss an estimate of upper (0–750 m) OHCA estimated from a combination of in situ temperature profiles with satellite altimetry sea surface height data for the period of 1 January–31 December 2006 (Fig. 3.3), analyzed following Willis et al. (2004), but relative to a 1993–2006 baseline. Data from Argo floats with a recently detected systematic bias in reported pressure values have been removed from the estimates discussed here. Details of the fields analyzed here may change after more real-time data are subject to delayed-mode scientific quality control.

The 2006 combined OHCA map (Fig. 3.3) shows eddy and meander variability down to the 100-km mapping scales, as does, to a greater extent, the difference between the 2006 and 2005 combined OHCA maps (Fig. 3.4). There is a great deal of small-scale spatial variability in OHCA fields associated with the western boundary currents in every gyre, as well as the Antarctic Circumpolar Current. The difference in combined OHCA maps between 2006 and 2005 (Fig. 3.4) illustrates the large year-to-year variability in ocean heat storage, with changes reaching or exceeding the equivalent of an 80 W m^{-2} magnitude surface flux. Ocean advection likely plays a significant role in many of these changes.

Large-scale patterns are also evident in OHCA for 2006 (Fig. 3.3), and for its difference from 2005 (Fig. 3.4). One of the prominent patterns is along the equatorial Pacific, where there is a band of high heat content in 2006, which is also seen as a heat gain since 2005. This pattern is consistent with the onset of El Niño in 2006. There is also a band of high OHCA along 10°N from the western Pacific to about 160°W. In addition, there is a band of high OHCA that reaches from 150°E on the equator to at least 120°W and about 25°S.

The combined OHCA map for 2006 (Fig. 3.3) is high in the subpolar North Atlantic (except for seas just northeast of Iceland) and low in the subtropical North Atlantic. This pattern dynamically implies a decreased strength of the North Atlantic Current, and is probably related to decadal changes in the North Atlantic Oscillation Index (e.g., Curry and McCartney 2001). This climate index was lower in 2006 than during the baseline period; it has trended lower from 1993 to 2006.

In the equatorial Indian Ocean, OCHA is low in the east and high in the west (Fig. 3.3), with interannual variations (Fig. 3.4) apparently contributing to this pattern. The southern subtropics of the Indian Ocean are generally high in OCHA, but changes since 2005 (Fig. 3.4) do appear to be a dominant contributor to this pattern.

In 2006, OHCA is high in the Southern Oceans in a belt located north of the Antarctic Circumpolar Current (Fig. 3.3), especially east of New Zealand in the South Pacific and between 30° and 45°S in the South Atlantic, but less perceptible in the south Indian Ocean. This change has recently been studied on decadal time scales in the South Pacific (Roemmich et al. 2007) and appears to be related to changes in the wind stress field associated with an increase in the Antarctic Oscillation index. This index reached a peak in 1999, fell into a shallow valley in 2002, and has been near neutral since then. Consistent with this neutrality, there is relatively little large-scale trend of OHCA between 2005 and 2006 in this region (Fig. 3.4), with smaller spatial scale changes of vary-

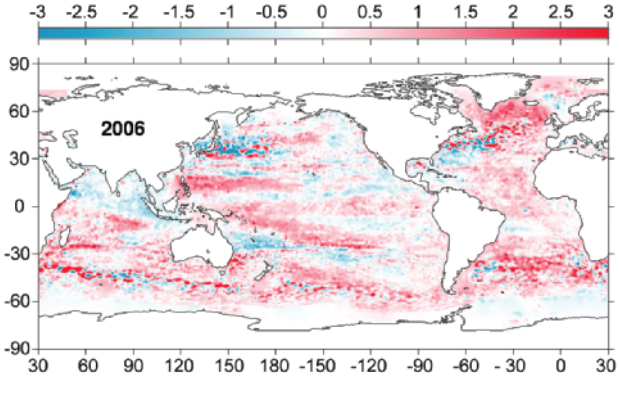

Fig. 3.3. Combined satellite altimeter and in situ ocean temperature data upper (0–750 m) ocean heat content anomaly OHCA (J m^{-2}) map for 2006.

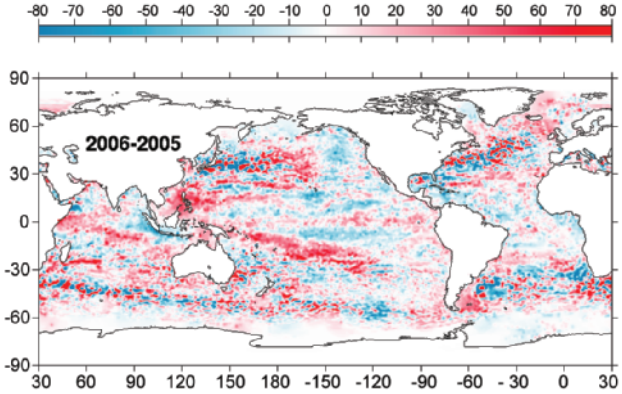

Fig. 3.4. The difference of 2006 and 2005 combined OHCA maps expressed as a local surface heat flux equivalent (W m^{-2}).

ing sign predominating in the subpolar regions of the Southern Hemisphere.

Finally, given the potential link between hurricane intensity and warm ocean waters (e.g., Emanuel 2005), we discuss tropical Atlantic patterns in OHCA. There was a record North Atlantic hurricane season in 2005 and a much weaker one in 2006 (see section 4). This change is consistent with decreases in OHCA from 2005 to 2006 in the Gulf of Mexico, in the Caribbean, and to a lesser extent around 10°N across much of the tropical North Atlantic (Fig. 3.4). This area had an increase in OHCA and hurricanes between 2004 and 2005 (Shein et al. 2006).

3) Global ocean heat fluxes—L. Yu and R. A. Weller

Latent heat (evaporation) and sensible heat fluxes are the primary mechanism by which the oceans release much of the absorbed solar energy back to the atmosphere. These ocean-to-atmosphere heat transfers are a cooling mechanism for the oceans but a source of heating for the atmosphere. The cooling and heating change the temperature gradients and energize the circulations in the ocean and atmosphere, which in turn affect air–sea temperature and humidity contrasts and modify the magnitudes of the ocean heat fluxes.

The estimates for the global LHF + SHF in 2006 (Fig. 3.5) were produced by the OAFlux project (Yu and Weller 2007) at the WHOI. The flux estimates are accurate within 8 W m^{-2}. On an annual mean basis, the largest absolute ocean heat losses occur over the regions associated with major WBCs and their extensions, the most noted of which are the Kuroshio off Japan, the Gulf Stream off the United States, and the Agulhas Current off the African coast. The magnitude of annual mean LHF + SHF in these regions exceeds 250 W m^{-2}, and is produced largely during the fall-to-winter seasons by strong winds and cold and dry air masses coming from the land. The secondary heat loss maximum (~180 W m^{-2}) is located over the broad subtropical southern Indian Ocean, where the large air–sea heat exchanges are sustained by the strong southeast trade winds during the boreal summer monsoon months (June–September).

Compared to the annual mean LHF + SHF in 2005 (Fig. 3.5), the heat fluxes in 2006 showed changes over all global basins, with the magnitude of the deviation within 50 W m^{-2}. Among all of the changes, two features in the tropical oceans are the most interesting. The first change is the increased LHF + SHF in the eastern and central equatorial Pacific Ocean concurrent with the development of a mild El Niño. In late 2006, SSTs were 2°–3°C above normal across much of the region. The increased evaporative heat loss is observed in regions of the El Niño warm SST anomalies. Variation of ocean heat fluxes in the tropical Pacific on ENSO time scales is a dominant interannual signal in the OAFlux multidecade time series (e.g., Yu and Weller 2007). The second feature is characterized by the east–west asymmetry in the 2005/06 difference anomalies in the tropical Indian Ocean. A positive IOD mode event occurred in 2006, with cold SST anomalies off the west coasts of Sumatra and Java and warm SST anomalies across the central and western parts of the basin. The IOD SST pattern is almost a mirror image of the El Niño SST in the Pacific. However, the changes in the flux patterns of these two basins did not mirror each other in 2006. The colder eastern Indian Ocean enhanced sea-to-air heat fluxes, while the warmer western Indian Ocean reduced the heat fluxes. This means that positive SST anomalies in the El Niño region correlated with positive heat flux anomalies, but positive SST anomalies in the Indian Ocean correlated with negative heat flux anomalies. The sign of the flux changes was opposite to the sign of the SST anomalies in the two basins, which suggested differ-

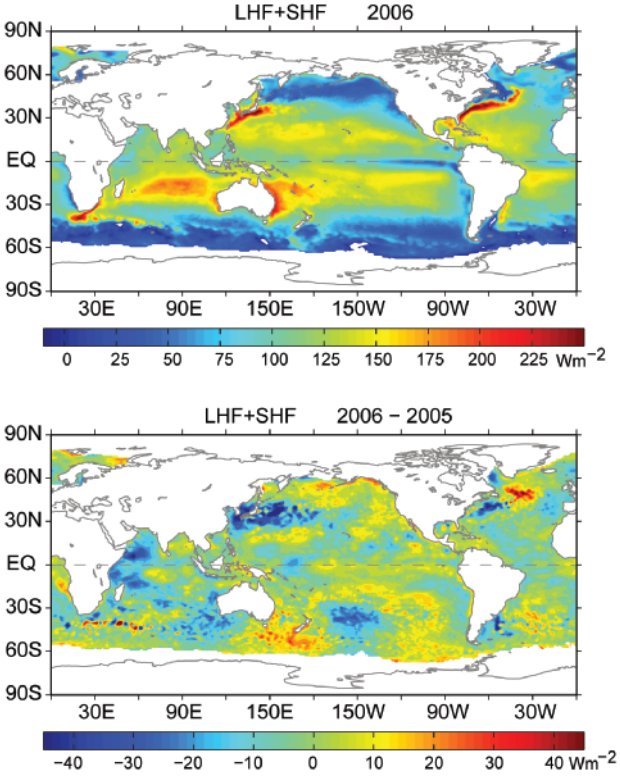

Fig. 3.5. (top) Annual mean latent plus sensible heat fluxes in 2006. The sign is defined as upward (downward) positive (negative). (bottom) Differences between the 2006 and 2005 annual mean latent plus sensible heat fluxes.